# Catalytic properties of $SrSn_{1-x}Sb_xO_3$ in methanol oxidation

H.R. Aghabozorg, B.H. Sakakini, A.J. Roberts, J.C. Vickerman and W.R. Flavell

*Department of Chemistry, UMIST, PO Box 88, Manchester M60 1QD, UK*

Received 27 April 1995; accepted 15 February 1996

Ceramic model catalyst materials of general formula $SrSn_{1-x}Sb_xO_3$ are synthesised by solid state reaction. X-ray diffraction shows the materials to be single phase over the composition range $0 \leqslant x \leqslant 0.085$, with a second phase, identified as $SrSb_2O_5$, being produced at higher antimony doping levels. XPS, Auger electron spectroscopy and valence band photoemission show strong segregation of Sb to the surface of the material even within the single phase regime. The catalytic properties of the materials are examined using methanol oxidation as a test reaction. The activity and selectivity to formaldehyde production shown by these materials is found to be strongly correlated with the attainment of the bulk solubility limit of Sb in the $SrSnO_3$ perovskite host.

**Keywords:** methanol oxidation; B-metal perovskites; $SrSn_{1-x}Sb_xO_3$

## 1. Introduction

Complex perovskite metal oxides are of considerable interest, as their properties may be tailored to specific applications by subtle changes in chemical doping at the A or B cation sites in the general formula $ABO_3$. This leads to applications in areas ranging from oxidation catalysis to superconductivity. In the former case, perovskites have normally been regarded as good deep oxidation catalysts. In the current work, our aim is to explore the extent to which the properties of certain catalytically active perovskites may be tailored by chemical doping in order to tune the behaviour of the material between deep oxidation and good selectivity to partial oxidation products. Our strategy has been to attempt to replicate the electronic and defect structure of a good partial oxidation catalyst, Sb-doped $SnO_2$ [1], inside the lattice of a perovskite material. The system we have chosen is $SrSn_{1-x}Sb_xO_3$, which we have shown to be broadly similar to $Sn_{1-x}Sb_xO_2$ in the general features of its band-structure [2]. There has been some recent interest in the action of similar perovskite and perovskite-related materials, containing heavy B-metal cations, such as Pb, Bi, Sn and Sb in the oxidative coupling of methane [3–5]. Here, we use the oxidation of methanol as a suitable test reaction for the system, and use the production of formaldehyde as a measure of selectivity to partial oxidation.

## 2. Experimental

Ceramic samples of nominal formula $SrSn_{1-x}Sb_xO_3$ ($0 \leqslant x \leqslant 0.5$) were prepared by solid state reaction. Stoichiometric amounts of $SrCO_3$, dry $SnO_2$ and $Sb_2O_3$ were ground to constant particle size in a ball mill, and the green mix was annealed in air at 1200°C for 12 h. After regrinding, the samples were reannealed at 1360°C for 60 h. In the case of samples used for XPS, pellets were pressed after the initial annealing cycle, and these were buried in powder of the same composition during the second annealing cycle, in order to reduce volatilisation of Sb from the discs [6].

X-ray diffraction (XRD) was carried out using a Scintag XDS2000 automated powder diffractometer and monochromated Cu K$\alpha$ radiation. SEM and energy dispersive X-ray analysis (EDAX) investigations were carried out for a range of samples using a Philips SEM505 microscope with a 9100/60 system attachment for EDAX. X-ray photoelectron spectroscopy (XPS) was carried out using a Fison's Instruments XR3 twin anode X-ray gun and CLAM2 hemispherical analyser, in an ion-pumped chamber. In this case, pelletised samples, mounted in molybdenum sample holders were used. Valence band photoemission measurements were carried out at the Synchrotron Radiation Source, CLRC Daresbury Laboratory, UK. These used the toroidal grating monochromator ($15 \leqslant h\nu \leqslant 90$ eV) and VG ADES 400 analyser on station 6.2. For these measurements, pelletised samples were mounted onto Mo sample plates using silver-loaded UHV-compatible epoxy resin. Auger electron spectra were recorded with a VSW EG5 electron gun and VSW HA50 hemispherical analyser, mounted in a diffusion-pumped chamber. Here the samples were mounted in a Ta sample holder, suspended from W wires. During these and other surface science measurements [2,7,8], data were recorded from as-presented surfaces, and following a number of surface treatments, including argon ion bombardment and scraping with a diamond file, with the aim of characterising the Sb distribution at the surface.

The surface areas of the catalysts were measured by the BET method using nitrogen. In the methanol oxidation studies, a continuous flow system was used. 1 g

quantities of catalyst were loaded onto glass wool in the reactor, which was located in a temperature controlled furnace. Methanol was introduced by bubbling dry He through a glass saturator filled with methanol. The flow rates of dry $O_2$, He/MeOH and He above the catalyst were controlled using a vent valve before the reactor and measured by a bubble flow meter after the reactor. The product gases were sampled immediately after the reactor, and were injected into a gas chromatograph provided with a TCD detector for analysis. $O_2$, $CO_2$, HCHO, $H_2O$ and MeOH were separated using a Propak-T column. To prevent condensation of reactant and product gases the tubing between the saturator and the sampling valve was heated to 373–383 K. The catalysts were pretreated at 723 K in 1 : 1 $He/O_2$ for 16 h, followed by flushing with He for 15 min. To investigate the effect of different pretreatments on the catalytic behaviour, catalysts were also pretreated in pure He at 723 K for 16 h. Reaction was carried out at temperatures in the range 563–638 K, and under conditions which limited the total conversion to less than around 10%. After establishing steady state conditions (around 30 min in reactant flow), the reaction products were analysed at a constant flow rate of 52 ml $min^{-1}$. For each catalyst material and each pretreatment, three experimental runs were made, and measurements were taken as the temperature was raised. In order to check that these measurements were not affected by any time-dependent poisoning effects, for selected materials the measurements were rechecked as the temperature was lowered. No significant changes were noted. In general, for each material tested the results from different experimental runs agreed to within the limits of experimental error. The error associated with the averaged readings taken for each sample is estimated to be $\leqslant \pm 3\%$. This gives relative errors in % selectivity and % total conversion (table 2) of $\leqslant \pm 5\%$.

## 3. Results and discussion

### 3.1. Bulk characterisation

After final annealing, the $SrSnO_3$ sample was white, but the Sb-doped samples were blue/grey, deepening in colour up to doping levels of around $x = 0.05$. Powder XRD patterns for various values of $x$ are shown in fig. 1. In the doping range $0 \leqslant x \leqslant 0.085$, the samples appeared single-phase [2], and the reflections were indexed using the standard JCPDS file (No. 22-1442) for $SrSnO_3$. The use of Si as an internal standard allowed the precise calculation of lattice parameters for the single perovskite phase, which showed a general decrease with increasing dopant concentration. For samples with doping levels $\geqslant 10$ at% a secondary phase, identified as $SrSb_2O_5$ was observed in amounts increasing with Sb-dopant concentration (fig. 1). While XRD is insensitive to the presence

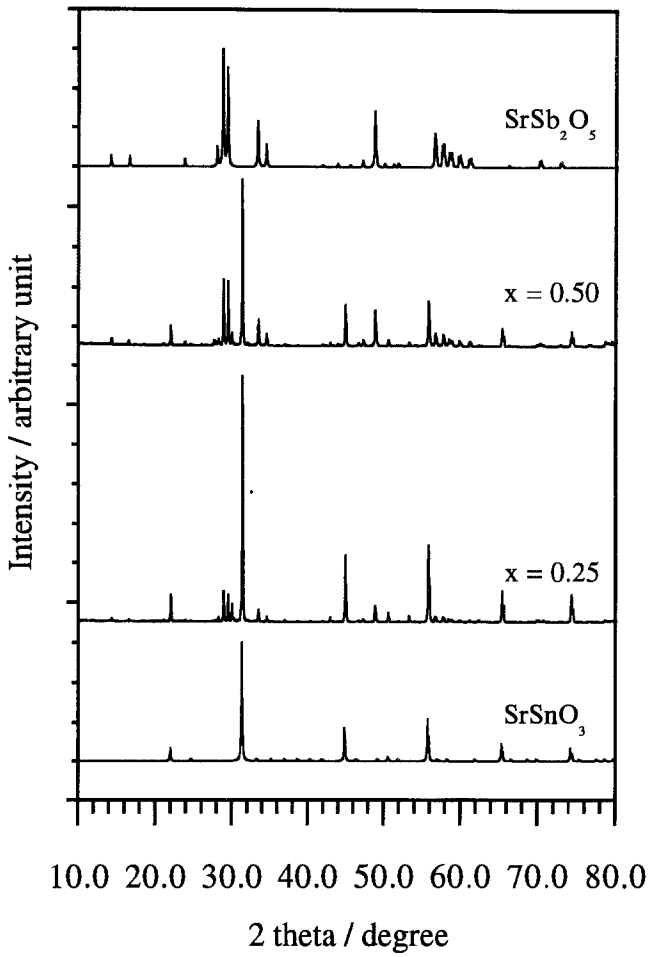


Fig. 1. Powder XRD patterns for $SrSnO_3$, $SrSn_{1-x}Sb_xO_3$ ($x = 0.25$ and $x = 0.50$), and $SrSb_2O_5$, showing the appearance of the second phase as a function of Sb doping level.

of a few percent of a second phase, it appears that the bulk solubility limit of Sb in this phase is around 8.5 at%. XRD patterns recorded before and after catalytic reaction showed that no discernible change in the proportion of the second phase had occurred during the reaction.

As might be expected from the high annealing temperatures used to synthesise these "model catalyst" materials, the samples were highly crystalline, as evidenced by the narrow reflections observed in XRD. The typical particle size in the sintered samples as observed in SEM was around 4 $\mu$m, and there was no obvious change in particle morphology on exceeding the bulk solubility limit [2]. Consistent with this, the BET surface areas were much lower than in a normal working catalyst material, typically in the range 0.3–0.6 $m^2\ g^{-1}$, and these showed small random fluctuations with Sb doping level. We note that the values obtained via this route for powders with surface areas $< 1\ m^2\ g^{-1}$ may be subject to errors of around ±25%, so these measurements suggest that the surface area of the materials may be regarded close to constant across the doping range. EDAX from a range of samples showed that the actual Sb doping levels

agreed with the nominal values to within the error limits of the technique; unfortunately, these are large relative to the Sb doping level for $x \leqslant 0.05$, making the analysis of limited usefulness in this range.

### 3.2. Surface characterisation

Our investigations of this system using surface science techniques have concentrated on the region of the phase diagram below the bulk solubility limit, where the samples are well-characterised single phase materials. The techniques applied to the system have included synchrotron-excited resonant photoemission [2,7,8], XPS [2,8], inverse photoemission [2,8], Auger electron spectroscopy [2,8] and electron energy loss spectroscopy [8]. As this work has been reported previously, we summarise these results only briefly here, concentrating on the techniques giving information about the distribution of Sb at the surface.

The surface chemical composition of as-presented samples was examined using XPS. In the carbon 1s region, this showed a signal attributable to hydrocarbon surface contamination, with a very small peak to high binding energy, indicating the presence of $SrCO_3$ [9]. Accelerated degradation testing of the samples (involving exposure to $CO_2$ in the presence of water vapour for extended periods) showed the samples to be extremely resistant to the formation of $SrCO_3$. (This contrasts, for example, with the behaviour of transition metal oxides containing alkaline earth ions, which tend to be rather susceptible to such reactions [9].)

Mg K$\alpha$ excited X-ray photoelectron spectra in the region of the Sn/Sb 3d core level ionisations for as-presented samples are shown in fig. 2. Although the Sb $3d_{5/2}$ peak overlaps with the O 1s peak, from comparison of the Sn $3d_{3/2}$ and Sb $3d_{3/2}$ peak intensities it is evident that there is pronounced surface enrichment in antimony over all compositions shown. This data is quantified in table 1, which also shows the surface composition obtained from integration of the less surface sensitive 4d peaks, and the MNN intensity ratio obtained in AES, again for as-presented samples. All data has been background subtracted, and in the case of photoemission, the data is additionally corrected for photoionisation cross section [10]. In the case of AES, the $I(\mathrm{Sb})/I(\mathrm{Sn})$ intensity ratios have been calculated from the peak-to-peak height of the $\mathrm{d}N(E)/\mathrm{d}E$ spectra. No absolute quantification of the Sb : Sn ratio at the surface is attempted from AES, due to uncertainties in cross sections. However, as the Auger transitions have similar energies and will be subject to similar backscattering effects, the intensity ratio may be used to give some general indication of the surface Sb : Sn ratio. Errors associated with the integrations are estimated at $\pm 10\%$. Also shown are values for photoelectron inelastic mean free pathlength, $\lambda$, relevant to the different experimental observations. We show estimated values from the "universal curve" for inorganic materials [11]. However, we note that the curve shows a wide scatter in this kinetic energy range. We believe that this approach may somewhat overestimate $\lambda$ in these materials, which contain heavy scatterers, and we note that the values calculated using the approach of Leckey and co-workers [12,13] (appropriate to electron kinetic energies > 300 eV) are rather smaller.

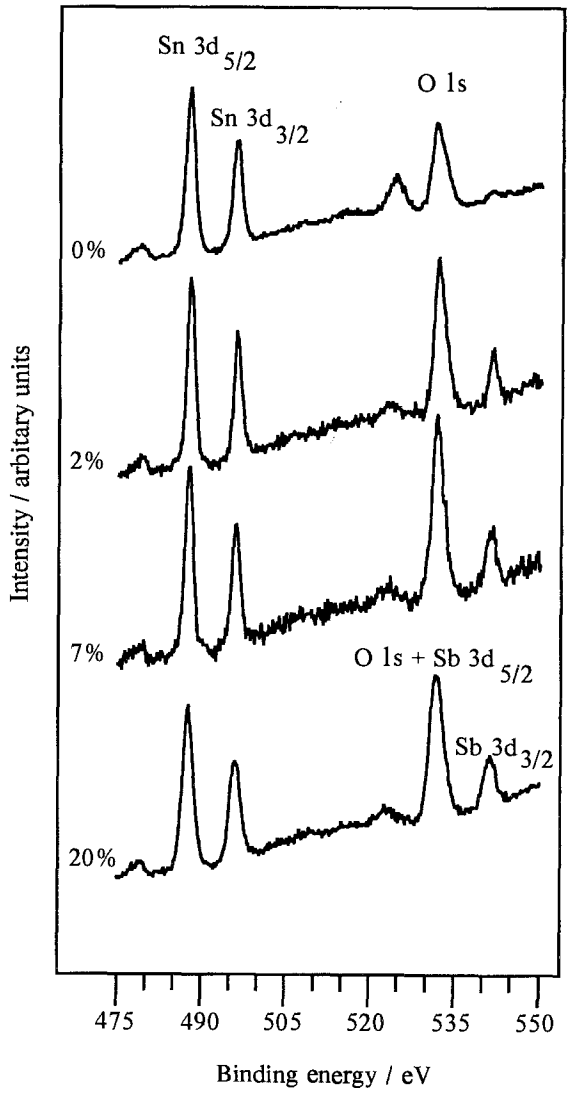


Fig. 2. Mg K$\alpha$ excited XPS of as presented $SrSn_{1-x}Sb_xO_3$, showing the Sn/Sb 3d and O 1s regions [2]. Surface segregation is evident from comparison of the relative intensities of the Sn $3d_{3/2}$ and Sb $3d_{3/2}$ peaks.

It is clear from the data for as-presented samples (table 1) that strong surface segregation of Sb is present. The surface experimental Sb : Sn ratio from XPS is up to 20 times higher than the bulk nominal ratio, and this is reinforced by AES, where significantly enhanced $I(\mathrm{Sb})/I(\mathrm{Sn})$ ratios are observed. Importantly, the values for the Mg K$\alpha$-excited 4d photelectrons appear lower than those for the 3d photoelectrons. The smaller surface Sb content obtained with longer $\lambda$ 4d photoelectrons shows that the depth of the segregated layer at the surface is probably of a similar order of magnitude to the

Table 1
The bulk nominal and experimentally determined surface concentration ratios $N(Sb)/N(Sn)$. Experimental values are calculated from the respective peak areas background subtracted, and (in the case of photoemission) corrected for photoionisation cross section

| Bulk nominal | | Surface experimental | | | | |
|---|---|---|---|---|---|---|
| $x$ | $N(Sb)/N(Sn)$ | $3d_{3/2}$ [a] | 4d [a] | AES [b] | AES [c] | 4d [d] |
| 0.005 | 0.005 | 0.05 | 0.05 | – | – | – |
| 0.02 | 0.020 | 0.41 | – | 0.32 | – | 0.14 |
| 0.05 | 0.053 | 0.42 | 0.27 | 0.48 | – | 0.21 |
| 0.07 | 0.075 | 0.46 | 0.37 | 0.68 | 0.10 | 0.30 |
| IMFP[11] [e] (Å) | | 25 | 50 | 20 | 20 | 10 |
| IMFP[12,13] [e] (Å) | | 15 | 22 | 10 | 10 | – |

[a] Peak areas determined from Mg Kα-excited XPS; as-presented samples.
[b] Experimental *intensity* ratio, $I(Sb)/I(Sn)$ from the respective MNN transitions in AES; as-presented samples.
[c] As b, after argon ion etching under the conditions given in the text.
[d] Peak areas determined from 70 eV synchrotron-excited photoemission spectra; after sample scraping using a diamond file.
[e] The photoelectron IMFP's estimated from the universal curve for inorganic compounds [11], and values calculated for photoelectron kinetic energy > 300 eV using the approach of Leckey et al. [12,13].

IMFP's. (In contrast, if the segregated layer was uniform and thick relative to the pathelength, we would not expect to see any variation in composition as a function of $\lambda$.)

In all cases the increase in surface Sb content on doping shows a smaller than linear variation with $x$. This is particularly marked in the case of the 3d ratios which vary only weakly between $x = 0.02$ and $x = 0.07$. Comparison of these with the 4d ratios obtained in the same experiment suggests that the Sb concentration in the topmost surface layers of the stannate may be approaching some limiting value when the bulk doping level reaches a few percent. In the subsurface layers, probably spanning several tens of Å into the surface, the Sb content is lower, but still enhanced over the nominal value, and increases somewhat with $x$.

Mild argon ion etching (500 eV/3–8 μA/8–10 min/$10^{-5}$ mbar argon) caused the complete removal of the segregated layer, and the Sb : Sn ratio returned to close to nominal (table 1) [2,8]. However, a rather different result was obtained on scraping away macroscopic quantites of the sample in UHV using a diamond file. Following this treatment, the levels of surface carbon contamination, as measured by AES and valence band photoemission, were greatly reduced, but some significant Sb segregation remained. This is shown in table 1, where the Sb : Sn ratios measured after sample scraping using the 4d levels excited by 70 eV synchrotron radiation are shown. The kinetic energy of the photoelectrons created here is only around 40 eV, giving a very surface sensitive measurement with an IMFP of only around 10 Å. The Sb : Sn ratios are clearly lower than those from the as-presented samples, but are still markedly higher (by a factor of 4–7) than the bulk nominal values, in contrast to the results obtained from etching. We believe that the contrast between the results from the two forms of sample treatment suggests that the Sb is segregated largely to grain boundaries in the sample. Cleaning using a diamond file results in significant areas of inter-, rather than intra-grain fracture [14], re-exposing new grain boundaries containing segregated Sb. In contrast, Ar bombardment may etch the surface more uniformly, or may even in some cases preferentially etch grain boundaries, thus removing the segregated layer [15].

Similar segregation has been reported in $BaSn_{1-x}Sb_xO_3$ [16], and in the partial oxidation catalyst $Sn_{1-x}Sb_xO_2$ [17,18]. In the latter case, at the bulk solubility limit of Sb in the $SnO_2$ lattice (around 3 at%), it is calculated that every surface Sn ion has been replaced by Sb [18]. Calcination of $Sn_{1-x}Sb_xO_2$ samples with a higher antimony content in air leads to loss of $Sb_2O_4$, and formation of Sb-doped $SnO_2$ with limiting composition $Sn_{0.97}Sb_{0.03}O_2$ [17,19]. Thus the observation of pronounced Sb segregation in the stannate is consistent with previous work on systems with related local structure (octahedral environment for Sn/Sb) and band structure.

### 3.3. Catalytic measurements

For each catalyst material, Arrhenius plots were constructed for partial (production of HCHO), deep (production of $CO_2$) and total ($CO_2$ + HCHO) oxidation, after He and $He/O_2$ pretreatments, over the temperature range 548–623 K. It was assumed that the rate law does not change with temperature or composition, so that the measured rate of production of products was taken as proportional to rate throughout. In general, good straight-line plots were obtained, allowing the extraction of activation energies for both partial and deep oxidation. For partial oxidation, these are typically in the range 20–50 kJ $mol^{-1}$, with higher values, in the range ~ 70–120 kJ $mol^{-1}$ for deep oxidation. In both cases, the activation energies rise to a maximum at around 7–10% Sb doping level, and then fall. The values for partial oxidation are low and indicate that the reaction is moving to deep oxidation at higher temperatures. This can be seen in table 2, which shows a compilation of % conversion and selectivity data for a range of the materials studied.

The total activity of the catalyst materials was not substantially affected by the pretreatment process used. Fig. 3 shows the activity of the catalyst materials to production of all products ($CO_2$ and HCHO) as a function of bulk antimony content after He pretreatment (temperature 580 K) and after $He/O_2$ pretreatment (temperature 578 K). The temperature chosen here is in the mid-range of those studied, and the data points are taken from the straight-line fits to the relevant Arrhenius plots.

Table 2
Selectivity to HCHO and total conversion in methanol oxidation over $SrSn_{1-x}Sb_xO_3$ as a function of Sb content, temperature and catalyst pretreatment, for selected representative compositions

| Sb (%) | T (K) | HCHO selectivity (%) | | Total conversion (%) | |
|---|---|---|---|---|---|
| | | $He/O_2$ pre. | He pre. | $He/O_2$ pre. | He pre. |
| 0 | 563 | 10.0 | 7.1 | 2.0 | 2.6 |
| | 578 | 6.2 | 4.6 | 3.2 | 4.0 |
| | 593 | 4.8 | 3.3 | 5.1 | 5.8 |
| | 608 | 3.5 | 2.4 | 7.3 | 7.6 |
| | 623 | 2.1 | 1.4 | 9.6 | 9.0 |
| | 638 | 1.3 | 1.0 | 12.0 | 9.8 |
| 7 | 563 | 19.0 | 26.5 | 0.4 | 0.3 |
| | 576 | 15.3 | 19.4 | 0.8 | 0.4 |
| | 593 | 13.5 | 19.3 | 0.9 | 0.7 |
| | 608 | 10.2 | 14.2 | 1.3 | 1.1 |
| | 623 | 9.5 | 8.9 | 1.8 | 1.7 |
| | 638 | 6.7 | 8.6 | 3.0 | 3.0 |
| 10 | 563 | 24.8 | 45.6 | 0.3 | 0.2 |
| | 578 | 19.5 | 28.1 | 0.6 | 0.4 |
| | 593 | 19.2 | 29.0 | 0.9 | 0.6 |
| | 608 | 13.8 | 20.8 | 1.7 | 1.1 |
| | 623 | 10.5 | 15.5 | 3.2 | 1.7 |
| | 638 | 9.4 | 13.7 | 4.5 | 2.6 |
| 20 | 548 | 11.0 | 15.2 | 0.4 | 0.2 |
| | 563 | 10.2 | 13.7 | 0.6 | 0.4 |
| | 578 | 6.0 | 8.5 | 1.2 | 0.7 |
| | 593 | 4.5 | 6.0 | 2.1 | 0.7 |
| | 608 | 3.2 | 3.7 | 3.2 | 2.4 |
| | 623 | 2.0 | 2.8 | 5.4 | 4.1 |
| 50 | 548 | 2.7 | 5.3 | 1.3 | 1.0 |
| | 563 | 2.0 | 3.7 | 2.4 | 1.9 |
| | 578 | 1.4 | 2.6 | 3.7 | 3.4 |
| | 593 | 1.0 | 2.4 | 6.7 | 4.9 |
| | 608 | 0.6 | 1.2 | 10.6 | 8.8 |
| | 623 | 0.3 | 0.6 | 13.1 | 13.1 |

Here, activity is normalised in the conventional way to the mass of catalyst, i.e. ln(mol $g^{-1}$ $min^{-1}$), but normalisation instead to the surface area of the catalyst produces an insignificant change to the overall shape of the plots, as the variations in surface area across the doping range are small and random. The effect of temperature on the activity/composition relationship is discussed further below.

Figs. 4 and 5 show the selectivity of the materials to the production of formaldehyde, again as a function of bulk antimony content after He pretreatment and $He/O_2$ pretreatment. The data in fig. 4 is presented in the conventional way, maintaining a roughly constant total conversion, while fig. 5 shows selectivity at a fixed low temperature of 563 K. The data is given for all temperatures sampled in table 2. It can be seen that, whilst the total conversion obtained from these very low surface area materials is always low, the selectivity of the materials to the production of formaldehyde varies dramatically with temperature and with antimony doping level, rising to 45% for the 10% Sb-doped sample (pretreated in He) at the lowest temperatures used.

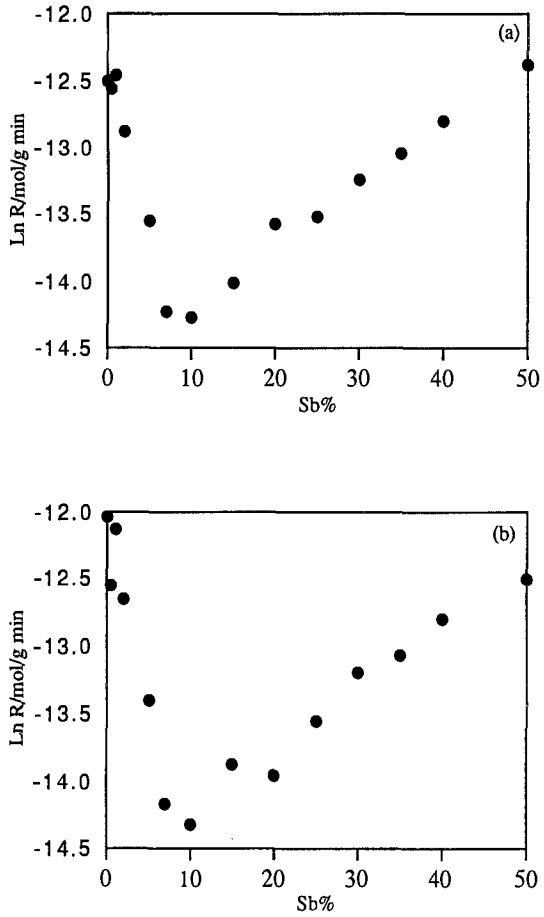


Fig. 3. The effect of Sb doping on catalyst activity in methanol oxidation (expressed as ln(total moles $g^{-1}$ $min^{-1}$)) (a) at 578 K after $He/O_2$ pretreatment, (b) at 580 K after He pretreatment.

A number of trends emerge from the data. The most dramatic of these, shown clearly in the data of fig. 3, and reflected in the data at other temperatures, is the drop in activity of the materials as Sb is introduced. This drop in overall activity of the materials is produced mainly by a drop in the rate of production of $CO_2$. At the lowest temperatures studied, the rate of production of total products decreases by over an order of magnitude between 0% and 7–10% doping levels. The activity then climbs again more slowly, through to the highest doping level studied. The activity minimum appears to correlate exactly with the bulk solubility limit of Sb in the $SrSn_{1-x}Sb_xO_3$ phase, which was earlier determined to be around 8.5 at% Sb [2]. Beyond this limit, increased activity is seen from catalysts which consist of mixed $SrSn_{1-x}Sb_xO_3$ and $SrSb_2O_5$ phases. XRD measurements taken before and after the catalytic reaction suggest that the overall phase composition of the catalyst is not changed by the reaction.

Selectivity to production of formaldehyde is highest at the lowest temperatures studied, and again appears to

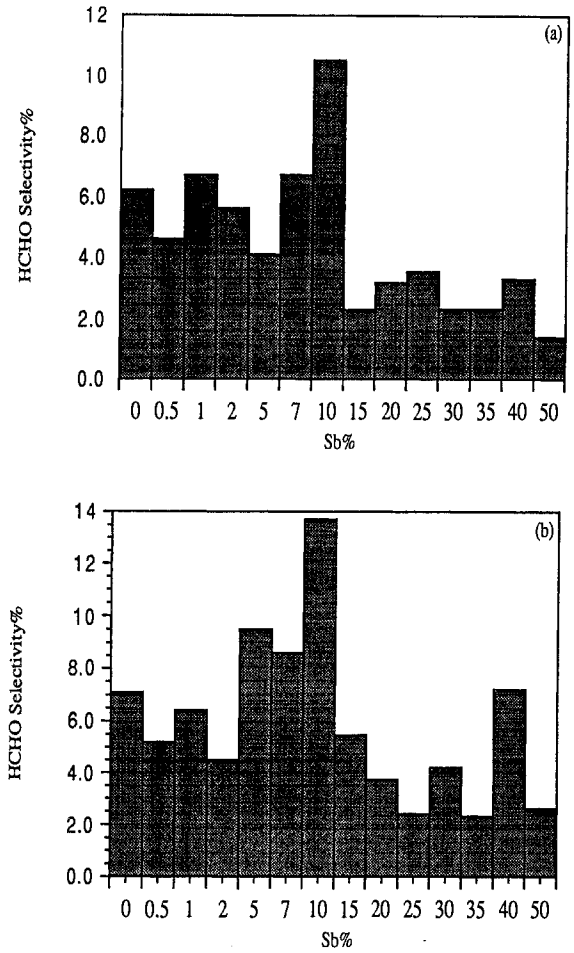


Fig. 4. The effect of Sb doping on catalyst selectivity to production of HCHO from methanol (at constant total conversion). (a) $He/O_2$ pretreatment, % conversion maintained in the range 2.5–4.2%, (b) He pretreatment, % conversion maintained in the range 2.4–3.7%.

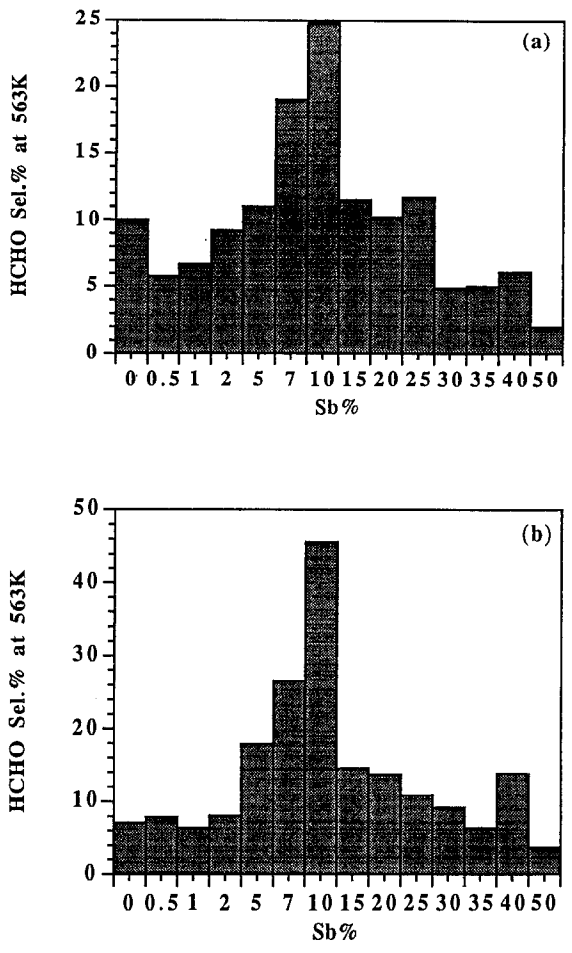


Fig. 5. The effect of Sb doping on catalyst selectivity to production of HCHO from methanol, at a fixed temperature of 563 K, emphasising the selectivity of the material at low temperature. (a) $He/O_2$ pretreatment, (b) He pretreatment.

show some correlation with antimony content, being highest in general for antimony contents in the range 7–10% Sb. Thus the materials appear to show optimum selectivity to HCHO when the overall activity of the catalysts is lowest, at around the bulk solubility limit of Sb in $SrSn_{1-x}Sb_xO_3$. This is enhanced at low operation temperatures, where the selectivity of the material rises to around 45% for He-pretreated materials. It can also be seen from fig. 5 that the selectivity of the He-pretreated materials at low temperatures appears significantly higher than that of the $He/O_2$-treated materials.

## 4. General discussion

The general form of the activity/composition curve for these materials, i.e. an initial fall followed by a rise, has been observed for a range of other doped oxide materials [20–23]. For example, the activity of model $Sn_{1-x}V_xO_2$ and $Ti_{1-x}V_xO_2$ catalysts in the decomposition of $N_2O$ follows a similar pattern [20]. This has been correlated with increases in the conductivity of the materials on doping [21]. In addition, it is suggested that high selectivity to partial oxidation products is correlated with the resulting relatively facile electron exchange between active site cations, combined with a high metal–oxygen bond strength (i.e. strongly bound oxygen) [21]. The latter property appears to be quite general to selective double oxide systems; for example the most selective systems show rather low rates of homomolecular isotopic oxygen exchange [24]. This can be rationalised on the basis of a Mars–van Krevelen type mechanism, where tightly bound nucleophilic lattice oxygen is responsible for production of selective oxidation products, whereas weakly bound, surface adsorbed electrophilic oxygen tends to lead to total oxidation [24].

We note some similarities between our system and the U–Sb oxide partial oxidation catalysts [25–29]. In this mixed phase system, high selectivity has been associated with the presence of $Sb^V$ ions in octahedral coordination, while the U centres in the material are thought to be responsible for formation of deep oxidation waste products [27]. A large increase in selectivity to formation

of acrylonitrile in propene ammoxidation is observed at a U : Sb ratio of 3 : 1 [25], associated with the formation of a $USb_3O_{10}$ phase [26–28]. The particularly high selectivity of this phase is thought to be due to its structure, which is such that the waste forming U centres are isolated from one another by Sb, and there are no adjacent U–O–U structures [28]. The success of the material in partial oxidation is therefore due to the presence of $Sb^V$ in octahedral coordination (which gives good selectivity), combined with isolation of centres for deep oxidation. The behaviour of the electrical conductivity of the system is complex, but is also thought to influence the catalytic properties [29].

In the light of the discussion above, it would seem that features which may give rise to high selectivity to partial oxidation in the stannate would be reasonable conductivity, combined with metal centres where O is strongly bound (possibly $Sb^V$), and isolation of deep oxidation centres. Based on these ideas, we consider a possible rationalisation of the behaviour of the system below.

$SrSnO_3$ is a wide band-gap insulator. As Sb has one more electron than Sn, each dopant ion introduced into the stannate should introduce a defect electron. In related materials, such as $Sn_{1-x}Sb_xO_2$, these defect electrons become itinerant at very low doping levels (estimated to be around 0.02% Sb doping), and a metallic metal oxide, displaying a finite density of states at the Fermi energy is produced [18]. In contrast, our photoemission measurements on $SrSn_{1-x}Sb_xO_3$ have shown that the defect electrons in this system do not become itinerant at any point across the solid-solution range (0–8.5% Sb) and a metallic material is not produced [2,7]. Nevertheless, introduction of Sb into $SrSnO_3$ has the overall effect of increasing the conductivity of the material in the single phase regime, as seen for example in the disappearance of charging effects in XPS with increasing doping level [2]. This suggests that a reasonably semiconducting material is produced. (Atomistic simulation calculations indicate that for the stannate a possible mode of defect electron compensation is through creation of Sr vacancies, which are formed readily within the stannate [30,31]. This mode of defect compensation is relatively common in perovskite structures.)

For the related system, $Sn_{1-x}Sb_xO_2$, the Sb present in the topmost surface layer of the material is thought to be present as $Sb^{III}$ [15]. This is produced by a slight reduction of the surface as oxygen at the predominant (110) faces of the ceramics is weakly bound and easily lost. However, Sb substitutes into the bulk of $SnO_2$ essentially as $Sb^V$, donating an electron to the conduction band. Consistent with this, Mössbauer results show the system to contain predominantly $Sb^V$, with $Sb^{III}$ present at the grain boundaries [32].

For $SrSn_{1-x}Sb_xO_3$, combined XANES (Sb $L_{III}$-edge) and EXAFS (Sb K-edge) results show Sb to be present in the bulk as $Sb^V$, with a typical $Sb^V$–O bond length of around 1.96 Å [8,33]. Mössbauer results for the related system $BaSn_{1-x}Sb_xO_3$ also show that bulk Sb is present at $Sb^V$ [34,35]. At the surface, we suppose that it may be also be possible for some reduced $Sb^{III}$ to be present, by analogy with $Sn_{1-x}Sb_xO_2$. If selectivity is associated with strongly bound oxygen, we might expect that, as the concentration of Sb in $SrSnO_3$ increases, the activity will drop, but the selectivity will increase, due to the replacement of Sn–O bonds (having a bond length of around 2.03 Å [8,33]) by very short and strong $Sb^V$–O bonds. We would in addition expect the selectivity to be highest for He-pretreated samples, as any loosely bound surface oxygen (associated with surface $Sb^{III}$), such as that seen in $Sn_{1-x}Sb_xO_2$, should be removed by this treatment. This is confirmed by the data of figs. 4 and 5.

Any effect on catalyst selectivity should be enhanced if Sb is segregated in the layers close to the surface. Our XPS data suggest that the surface layers of the material are strongly enriched in Sb at dopant levels below the bulk solubility limit, and that this segregation extends further into the bulk than just the topmost surface layer; certainly over several tens of angstroms from the surface. We would therefore expect the introduced $Sb^V$–O bonds to influence the selectivity strongly. It is well established that in even quite selective catalysts, oxygen exchange with the surface may occur over several tens or even hundreds of oxide layers [24]. (Ten oxide layers in this case corresponds to around 20 Å.) Thus it seems possible that the increase in selectivity and drop in activity in these materials between 0 and 10% Sb doping levels is related to the increasing concentration of $Sb^V$–O bonds in the first few tens of angstroms from the surface. However, we note from XPS that the Sb concentration in the surface layers varies relatively weakly with $x$, particularly in the range $x = 0.02$–$0.07$, where the activity and selectivity changes dramatically. The increasing amounts of $Sb^V$ alone may not be sufficient to explain this variation. It may be possible that the increasing levels of Sb in the surface layers are also simultaneously isolating the centres producing deep oxidation, as in $USb_3O_{10}$ [25–28]. This would result in an increase in selectivity, combined with a decrease in overall activity, produced by a drop in the rate of production of $CO_2$.

The activity minimum is correlated with the appearance of a second phase, $SrSb_2O_5$, produced beyond around 10 at% doping. This is a mixed valence material, which contains $Sb^{III}$ and $Sb^V$ valencies. We might expect weakly bound oxygen, such as that associated with $Sb^{III}$–O bonds to give rise to increased activity and to deep oxidation. Thus we associate the increase in activity and decrease in selectivity at $> 10\%$ doping with the presence of increasing numbers of $Sb^{III}$–O bonds in the surface regions, produced by the increasing proportion of the second phase $SrSb_2O_5$.

## 5. Conclusions

The activity and selectivity in methanol oxidation of this stannate catalyst may be tuned to some extent by varying the Sb doping level. The solubility limit of Sb in the phase is around 8.5 at%, and at the highest doping levels attainable within the single phase regime, the selectivity to production of HCHO rises to 25–45% (depending on pretreatment) at low operating temperatures. This represents quite a substantial yield of partial oxidation product for a perovskite material, and we are currently working to enhance this further by the addition of other co-dopants.

The activity of the material shows a pronounced minimum at around the solubility limit of Sb, and the activity/composition relationship is strikingly similar to those observed for other doped oxide materials. We suggest that the minimum in activity and maximum in selectivity is associated with a maximum in the concentration of $Sb^V$–O bonds in the surface regions at around 10 at% Sb doping. The high levels of Sb in the surface regions may also be sufficient to have a significant effect in isolating the deep oxidation centres, as in $USb_3O_{10}$ [27,28]. This is combined with an increase in the electronic conductivity of the material as Sb is added, such that the material at 10% doping level combines centres of high metal–oxygen bond strength with quite high electron mobility, both important properties for high selectivity [21].

XPS shows pronounced surface segregation of Sb in this system (in the solid solution range). In this respect, the system is very similar to $Sn_{1-x}Sb_xO_2$ which is an efficient partial oxidation catalyst [1]. By recreating within a perovskite lattice the basic features of the electronic structure of $Sn_{1-x}Sb_xO_2$, and its segregation characteristics, we have been able to tailor the behaviour of the stannate from almost complete deep oxidation in $SrSnO_3$ to over 45% partial oxidation for the Sb-doped material.

## Acknowledgement

This work was funded by EPSRC and the Royal Society.

## References

[1] K. Wakabayashi, Y. Kamiya and H. Ohta, Bull. Chem. Soc. Japan 40 (1967) 2172.
[2] A.J. Roberts, W.R. Flavell, D.R.C. Hoad, R.G. Egdell, S. Randall, P.L. Wincott and D. Teehan, Surf. Sci. 311 (1994) 181.
[3] D. Dissanayake, K.C.C. Kharas, J.H. Lunsford and M.P. Rosynek, J. Catal. 139 (1993) 652.
[4] P.D. Battle, S.W. Carr, F.A. Copplestone and S.A. Almaer, J. Chem. Soc. Chem. Commun. (1992) 826.
[5] P.D. Battle, S.W. Carr, F.A. Copplestone and R.S. Mellen, J. Mater. Chem. 4 (1994) 421.
[6] R.J. Cava, P. Gammel, B. Batlogg, J.J. Krajewski, W.F. Peck, L.W. Rupp, R. Fielder and R.B. van Dover, Phys. Rev. B 42 (1990) 4815.
[7] W.R. Flavell, D.R.C. Hoad, M. Mian, B.C. Morris, A.J. Roberts, M.M. Sarker, P.L. Wincott, D. Teehan and P. Bailey, Surf. Sci. 307–309 (1994) 1166.
[8] A.J. Roberts, PhD Thesis, UMIST, UK (1995).
[9] M.S. Golden, D.A. Geeson, S.E. Male and W.R. Flavell, Supercond. Sci. Technol. 2 (1989) 185.
[10] J.J. Yeh and I. Lindau, Atomic Data and Nuclear Data Tables 32 (1985) 1.
[11] M.P. Seah and W.A. Dench, Surf. Interf. Anal. 1 (1979) 2.
[12] J. Szajman and R.C.G. Leckey, J. Electron Spectrosc. Relat. Phenom. 23 (1981) 83.
[13] J. Szajman, J. Liesegang, J.G. Jenkin and R.C.G. Leckey, J. Electron Spectrosc. Relat. Phenom. 23 (1981) 97.
[14] J.A. Yarmoff, D.R. Clarke, W. Drube, U.O. Karlsson, A. Taleb-Ibrahimi and F.J. Himpsel, Phys. Rev. B 36 (1987) 3967.
[15] D. Briggs and M.P. Seah, eds., *Auger and X-ray Photoelectron Spectroscopy*, Practical Surface Analysis, Vol. 1 (Wiley, New York, 1990).
[16] R. Claessen, M.G. Smith, J.B. Goodenough and J.W. Allen, Phys. Rev. B 47 (1993) 1788.
[17] Y.M. Cross and D.R. Pyke, J. Catal. 58 (1979) 61.
[18] R.G. Egdell, W.R. Flavell and P.J. Tavener, J. Solid State Chem. 51 (1984) 345.
[19] D.R. Pyke, R. Reid and R.J.D. Tilley, J. Chem. Soc. Faraday Trans. I 76 (1980) 1174.
[20] P. Pomonis and J.C. Vickerman, J. Catal. 90 (1984) 305.
[21] P. Pomonis and J.C. Vickerman, J. Catal. 55 (1978) 88.
[22] P. Pomonis and J.C. Vickerman, Faraday Discuss. Chem. Soc. 72 (1981) 247.
[23] J.C. Vickerman, in: *Catalysis*, Vol. 2, eds. C. Kemball and D.A. Dowden, Specialist Periodical Report (Chemical Society, London, 1978) p. 107.
[24] A. Bielanski and J. Haber, *Oxygen in Catalysis* (Dekker, New York, 1991) pp. 132–155, and references therein.
[25] R.K. Grasselli and J.L. Callahan, J. Catal. 14 (1969) 93.
[26] R.K. Grasselli, D.D. Suresh and K. Knox, J. Catal. 18 (1970) 356.
[27] R.K. Grasselli and D.D. Suresh, J. Catal. 25 (1972) 273.
[28] R.K. Grasselli and J.D. Burrington, Adv. Catal. 30 (1981) 133.
[29] J.-M. Herrmann, J. Disdier, F.G. Freire and M.F. Portela, J. Chem. Soc. Faraday Trans. 91 (1995) 2343.
[30] R.I. Hines, N.L. Allan and W.R. Flavell, J. Chem. Soc. Faraday. Trans., submitted.
[31] R.I. Hines, N.L. Allan and W.R. Flavell, Phil. Mag., in press.
[32] F.J. Berry and C. Greaves, J. Chem. Soc. Dalton Trans. (1981) 2447.
[33] W.R. Flavell, M. Mian, A.J. Roberts, J.F. Howlett, Md.M. Sarker, P.L. Wincott, R.L. Bilsborrow, and G. van Dorssen, J. Mater. Chem., to be submitted.
[34] M. Eibschutz, R.J. Cava, J.J. Krajewski, W.R. Peck and W.M. Reiff, Appl. Phys. Lett. 60 (1992) 830.
[35] M.G. Smith, J.B. Goodenough, A. Manthiram, R.D. Taylor, W. Peng and C.W. Kimball, J. Solid State Chem. 98 (1992) 181.